An efficient photocatalytic system under visible light: in-situ growth cocatalyst Ni_2P on the surface of CdS

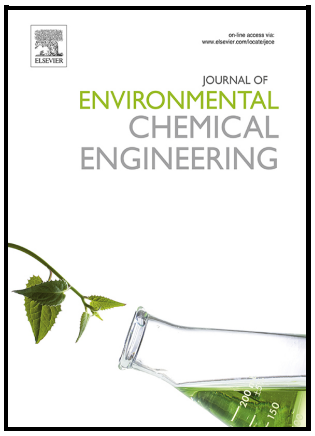

Wangyang Ma, Dewen Zheng, Bihua Xiao, Yuxi Xian, Qian Zhang, Shanyu Wang, Jin Liu, Ping Wang, Xianhai Hu

PII: S2213-3437(22)00695-9

DOI: https://doi.org/10.1016/j.jece.2022.107822

Reference: JECE107822

To appear in: *Journal of Environmental Chemical Engineering*

Received date: 8 February 2022
Revised date: 7 April 2022
Accepted date: 27 April 2022

Please cite this article as: Wangyang Ma, Dewen Zheng, Bihua Xiao, Yuxi Xian, Qian Zhang, Shanyu Wang, Jin Liu, Ping Wang and Xianhai Hu, An efficient photocatalytic system under visible light: in-situ growth cocatalyst Ni_2P on the surface of CdS, *Journal of Environmental Chemical Engineering,* (2022) doi:https://doi.org/10.1016/j.jece.2022.107822

An efficient photocatalytic system under visible light: in-situ growth cocatalyst Ni_2P on the surface of CdS

Wangyang Ma[a], Dewen Zheng[c] , Bihua Xiao[a], Yuxi Xian*[b], Qian Zhang[c], Shanyu Wang[c],Jin Liu[a], Ping Wang[a], Xianhai Hu*[a]

[a]Anhui Key Laboratory of Advanced Building Materials, School of Materials Science and Chemical Engineering, Anhui Jianzhu University, Hefei 230601, China

[b]University of Science and Technology of China, Hefei 230026, China

[c]New Energy Research Center Research Institute of Petroleum Exploration and Development (RIPED), Beijing 10083, China

ABSTRACT:

Cocatalyst contributes to promote the separation and transfer of charge in photocatalytic system, which is an important factor to improve photocatalytic decomposition of water to produce hydrogen. Here, a simple and effective method to combine the main catalyst and the cocatalyst by a modified impregnation method is provided. A novel Ni_2P/CdS is prepared by in-situ growth of Ni_2P cocatalyst on the CdS surface using the modified impregnation method. The research shows that Ni_2P, as an electron carrier, can promote the separation of electrons and holes, and significantly improve the photocatalytic activity of Ni_2P/CdS. When Ni_2P was 3% in Ni_2P/CdS, the photocatalytic activity of hydrogen production was the highest, and the hydrogen production rate reached an astonishing 16.02 mmol $h^{-1}g^{-1}$ under visible light, which was 57 times that of CdS. Moreover, Ni_2P/CdS photocatalyst has outstanding stability for hydrogen production. The mechanism of photocatalytic hydrogen production by Ni_2P/CdS is proposed.

Keywords: Photocatalysis, Hydrogen evolution, CdS, Ni_2P, Cocatalyst

1.Introduction

The hydrogen energy is an environment-friendly new energy carrier, which effectively solves the problems of environmental pollution and energy shortage caused by fossil fuels. Developing a sustainable and economical photocatalytic hydrogen production system is considered as the most promising way at present [1-3]. Photocatalytic decomposition of water not only makes effective use of solar energy, but also has low cost and sustainability [4-6].

Semiconductor photocatalysts such as TiO_2, CdSe and g-C_3N_4 have been reported [7-11]. Although they have a certain ability of photocatalytic decomposition of water, the efficiency of hydrogen production is very low due to the rapid recombination of electrons and holes [12, 13]. As a semiconductor material that can respond under visible light, CdS (2.4 eV) is considered as an ideal photocatalytic material with abundant and effective active sites and excellent conduction band positions [14-16]. However, CdS is prone to photocorrosion under light, and the separation efficiency of photogenerated carriers is low, resulting in low hydrogen production efficiency in practical application [17]. In the field of photocatalysis, loading effective cocatalyst can capture photoinduced charge and provide abundant active sites for surface Redox reaction, which is one of the most promising methods to improve the performance of photocatalysis [18-20].

Traditional cocatalysts are mainly precious metals such as platinum and gold, which are limited by high cost and rarity [21, 22]. At present, the research on metal oxides, hydroxides, sulfides and phosphides as substitutes of precious metals has been extensively reported [23-26]. Among them, transition metal phosphides (TMPs) are considered as efficient and stable hydrogen evolution promoters such as Ni_2P, CoP, FeP and MoP due to their low overpotential and excellent conductivity [27-30]. TMPs can be regarded as doping phosphorus (P) atoms into the crystal

lattice of transition metals [31]. Ni_2P is an interstitial compound formed by inserting P atoms into the nickel lattice, which has unique photoelectric properties and long-term stability, and is considered as one of the most important materials to replace precious metals as co-catalysts [32-34]. The conventional photocatalytic system of Ni_2P is the solid reaction of nickel salt with excess P or NaH_2PO_2 at high temperature (above 200 ℃) in an inert atmosphere to produce Ni_2P [35]. The performance of TMPs as cocatalyst mainly depends on the contact quality and area of photocatalyst on its surface [36-38]. Generally, Ni_2P and photocatalyst prepared by simple mechanical mixing have low separation efficiency of electrons and holes and low photocatalytic efficiency due to loose contact [39].

Herein, a new method to combine the main catalyst and the cocatalyst by a modified impregnation method was provided. The in-situ growth of Ni_2P on CdS surface is conducive to closer contact between Ni_2P and CdS surface using the modified impregnation method, which can effectively promote the separation of photogenerated electrons and holes, showing a more efficient performance of photocatalytic hydrogen production. Compared with the traditional preparation method combining TMPs and cocatalyst, the modified impregnation method greatly improves the catalytic activity of photocatalyst through close contact between the main catalyst and the cocatalyst. Compared with CdS nanorods, Ni_2P/CdS shows higher photocatalytic hydrogen production efficiency under visible light.

2. Experimental Section

2.1 Materials

Thiourea (NH_2CSNH_2, 99%), ethylenediamine ($NH_2CH_2CH_2NH_2$, 99%), methanol (CH_3CH_2OH, 99.7%), Na_2S (98%) and Na_2SO_3 (98%) were all purchased from sinopharm chemical reagents Co., Ltd. Cadmium chloride ($CdCl_2·2.5H_2O$, 98%) and nickel chloride hexahydrate ($NiCl_2·6H_2O$, 99%) were all purchased from Shanghai

McLean Biochemical Technology Co., Ltd. All are analytic reagent and used as received.

2.2 Preparation of CdS

CdS was prepared by solvothermal method [40]. $CdCl_2 \cdot 2.5H_2O$ and NH_2CSNH_2 were dissolved in $NH_2CH_2CH_2NH_2$ and stirred to form a homogeneous solution. Then the mixtures were transferred into Teflon-lined stainless-steel autoclave. The autoclave was heated at 160 °C for 48 h a hot air oven and then naturally cooled to room temperature. The products were clean with purified water and ethanol several times. Finally, it was dried at 80 °C for 8 h to obtain CdS.**2.3 Preparation of Ni_2P/CdS**

$NiCl_2 \cdot 6H_2O$ and NaH_2PO_2 were dissolved in purified water and stirred to form a homogeneous solution. CdS was added to the solution and ultrasonicated for 1 h. The mixtures were dried in the oven, and water was fully dried. It was heated to 300°C in a tubular furnace under N_2 for 1 h, and then cooled naturally to room temperature. The products were washed three times with ultra-pure water and anhydrous ethanol respectively. Finally, it was dried at 60 °C for 12 h to obtain Ni_2P/CdS. The 2%, 3%, 5%, 7% Ni_2P content of Ni_2P/CdS and Ni_2P were prepared by themethod, as shown for different contents ratios in Table 1. Scheme 1 is a schematic diagram of material preparation. Meanwhile, 100 mg of CdS was dispersed in 10 ml of ethanol, and ultrasonic treatment was carried out for 30min. With stirring, 3 mg of Ni_2P was added to the CdS suspension. The mixture was ultrasonically treated for 1 h, stirred for another 12 h, separated by centrifugation and washed with ethanol. Finally, the mixture was dried at 80℃ for 12 h to obtain 3% Ni_2P/CdS mechanical mixed photocatalyst.

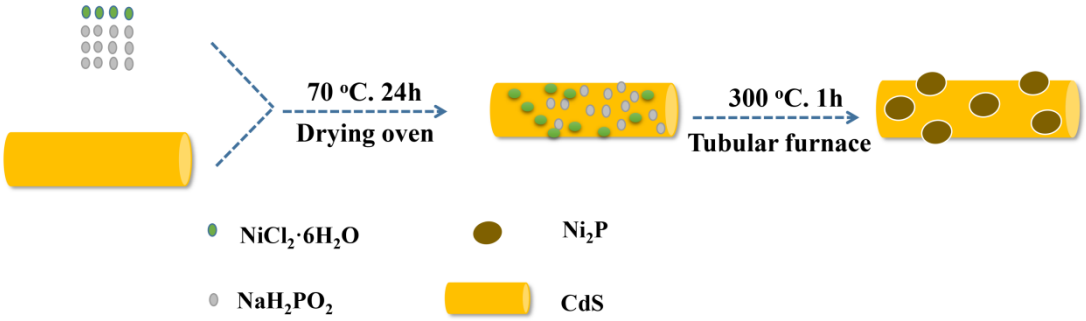

Scheme 1. Schematic diagram of one-step synthesis of Ni_2P/CdS.

Table 1. The ratio of Ni_2P and CdS in different content

Samples	$NiCl_2·6H_2O$ (mg)	NaH_2PO_2 (mg)	CdS (mg)
Ni_2P	200	1000	0
2% Ni_2P/CdS	19.2	96	300
3% Ni_2P/CdS	28.8	144	300
5% Ni_2P/CdS	48	240	300
7% Ni_2P/CdS	67.3	336.5	300

2.4 Materials characterization

X-ray diffraction spectrometer (XRD, SmartLab 9KW Japan) was used to analyze the crystal structure of photocatalyst. The microstructure of photocatalyst was analyzed by field emission scanning electron microscope (SEM, GeminiSEM 500 Germany), transmission electron microscope (TEM, JEM-2011 Japan) and high resolution transmission electron microscope (HRTEM, Talos F200X USA). Photoluminescence spectra of the samples were obtained at room temperature using a spectrometer (PL, F-4700 Japan). X-ray photoelectron spectroscopy (XPS, ESCALAB 250Xi, USA) was used to analyze the surface chemical state and the existing forms of elements of the composite photocatalyst, and the binding energy was calibrated with the signal of carbon at 284.8 eV as a reference. The adsorption-desorption isotherm of nitrogen was measured by Autosorb-iQ instrument and analyzed by Bruner-emmett-Taylor equation. Barrett joiner-Harunda (BJH) analytical aperture. Ultraviolet-visible diffuse reflectance spectrum was measured by

ultraviolet-visible spectrophotometer (UV-vis DRS, Solid Spec 3700, Japan), with Ba_2SO_4 as reference. Optoelectronic properties of samples were measured on an electrochemical analyzer (CHI 660E, China) with a standard three-electrode system. The Ag/AgCl is used as reference electrode, the counter electrode is Pt plate, and the working electrode is FTO coated with photocatalyst. Transient photocurrent response and electrochemical impedance were measured using 0.5 M Na_2SO_4 as electrolyte solution.

2.5 Photocatalytic Hydrogen Production

Photocatalytic hydrogen generation experiments were carried out in a photocatalytic activity evaluation system (MC-SPH_2O-A, China). 20 mg of catalyst was added into 50 ml of aqueous solution of 0.35 M Na_2S and 0.25 M Na_2SO_3, and the photocatalyst was dispersed evenly by ultrasonic for 15 min. Then, the air in the whole system was replaced by nitrogen circulation and degassed for 30 minutes to remove the air. The enclosed glass instrument was completely evacuated and irradiated with 300W Xe lamp with cut-off filter (λ > 420nm) (AuLight, CEL-HXF300) at room temperature to simulate the reaction initiated by sunlight for 4 h. The generated H_2 was analyzed by an online gas chromatograph (GC-7920, TCD) using high-purity nitrogen as carrier gas and oxygen as power gas.

3. Results and discussion

3.1. Characterization of Ni_2P/CdS composite

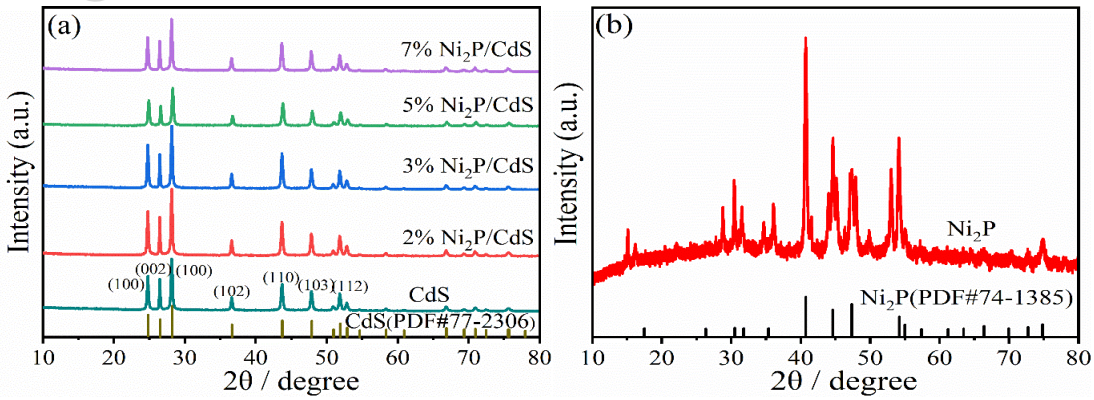

Fig. 1. (a) XRD patterns of CdS and (b) (2%, 3%, 5%, 7%) Ni_2P/CdS.

The XRD patterns of CdS, Ni_2P and Ni_2P /CdS with different Ni_2P amounts are illustrated in Fig. 1. Fig. 1 (a) shows that the X-ray diffraction peak of CdS is consistent with that of CdS (PDF#77-2306) There are strong diffraction peaks at 24.69, 26.35, 28.19, 36.59, 43.68, 47.79 and 51.82, which correspond to (100), (002), (101), (102), (110), (103) and (112) of CdS, respectively [41]. It shows that CdS with good crystallinity was synthesized by solvothermal method. The XRD pattern of Ni_2P/CdS has not changed, and the peak of Ni_2P has not been observed, which may be attributed to the low loading or high dispersion of Ni_2P, which will not change the crystal structure of CdS. All the diffraction peaks of Ni_2P/CdS are consistent with the XRD pattern of CdS, indicating that Ni_2P synthesis does not change the lattice structure of CdS. It can be seen from Fig. 1(b) that the X-ray diffraction peak of Ni_2P is consistent with that of Ni_2P (PDF#74-1385), and Ni_2P has a higher diffraction peak, illustrating that Ni_2P with high crystallinity was synthesized by impregnation method.

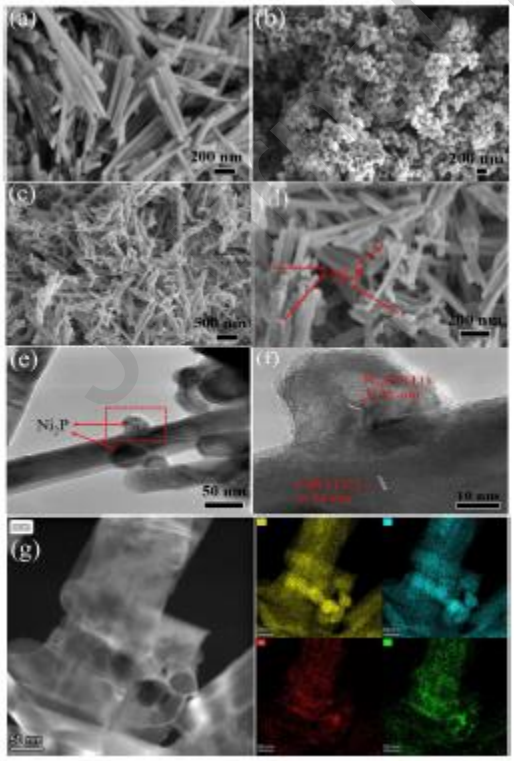

Fig. 2. (a) SEM image of CdS, (b) Ni_2P, (c-d) 3% Ni_2P/CdS at different magnifications and (e) TEM image of 3% Ni_2P/CdS, (f) HRTEM image of 3% Ni_2P/CdS, (g) SEM image of 3% Ni_2P/CdS and corre-sponding elemental mapping of Cd, S, Ni and P.

SEM, TEM and HRTEM of CdS and Ni_2P/CdS are shown in Fig. 2. In Fig. 2 (a), CdS can be clearly seen as smooth rod-like structures with average particle sizes of approximately 600 nm in length and 50 nm in width. Fig.2 (b) shows that Ni_2P has a spherical granular structure on its surface. Fig. 2 (c) and (d) are SEM of 3% Ni_2P/CdS. It can be observed that the surface of CdS nanorods is relatively rough, which is attributed to Ni_2P deposition on the surface of CdS nanorods. Granular Ni_2P can be clearly seen on CdS nanorods in Fig. 2 (e). It can be identified from Fig. 2 (f) and Fig. 2 (e) that the lattice fringes of 0.22 nm and 0.34 nm correspond to the (111) plane of Ni_2P and the (111) plane of CdS respectively, confirming that the particles are Ni_2P and grow on the CdS nanorods. Fig. 2 (g) is the elemental map of 3% Ni_2P/CdS, and it can be seen that elements Cd and S basically have the same elemental profile, and Ni and P are mainly concentrated in the spherical granular morphology, which further confirms that the spherical particles are Ni_2P, indicating that Ni_2P/CdS has been successfully synthesized.

X-ray photoelectron spectroscopy (XPS) of CdS and 3% Ni_2P/CdS are obseved in Fig. 3. Fig. 3 (a) shows the XPS spectrum, and it is observed that the main elements in CdS are cadmium and sulfur, and the main elements in 3% Ni_2P/CdS are cadmium, sulfur, nickel and phosphorus. The spectrum shows two peaks of 404.56 eV and 411.26 eV in Fig. 3(b), and the positions of CdS and 3% Ni_2P/CdS peaks are basically the same, which are attributed to Cd $3d_{5/2}$ and Cd $3d_{5/2}$, respectively [42]. Fig. 3(c) shows two peaks of 160.81 eV and 162.06 eV of 3% Ni_2P/CdS, and their positions are basically consistent with those of CdS, which are respectively attributed to S $2p_{3/2}$ and S $2p_{1/2}$ [43]. Fig. 3(d) demonstrates two peaks located at 853.46 eV, 856.26 eV and 861.76 eV, which are ascribed to $Ni^{\delta+}$, Ni $2p_{3/2}$ and Ni $2p_{1/2}$, respectively, indicating that Ni mainly exists in the form of Ni^{+2} [44, 45]. Fig. 3(e) displays the high-intensity diffraction peak at 133.16 eV, which belong to P $2p_{3/2}$, indicating that P mainly exists in the state of binding with Ni [46]. XPS results further confirmed that there is a mixture of Ni_2P and CdS in the photocatalyst Ni_2P/CdS.

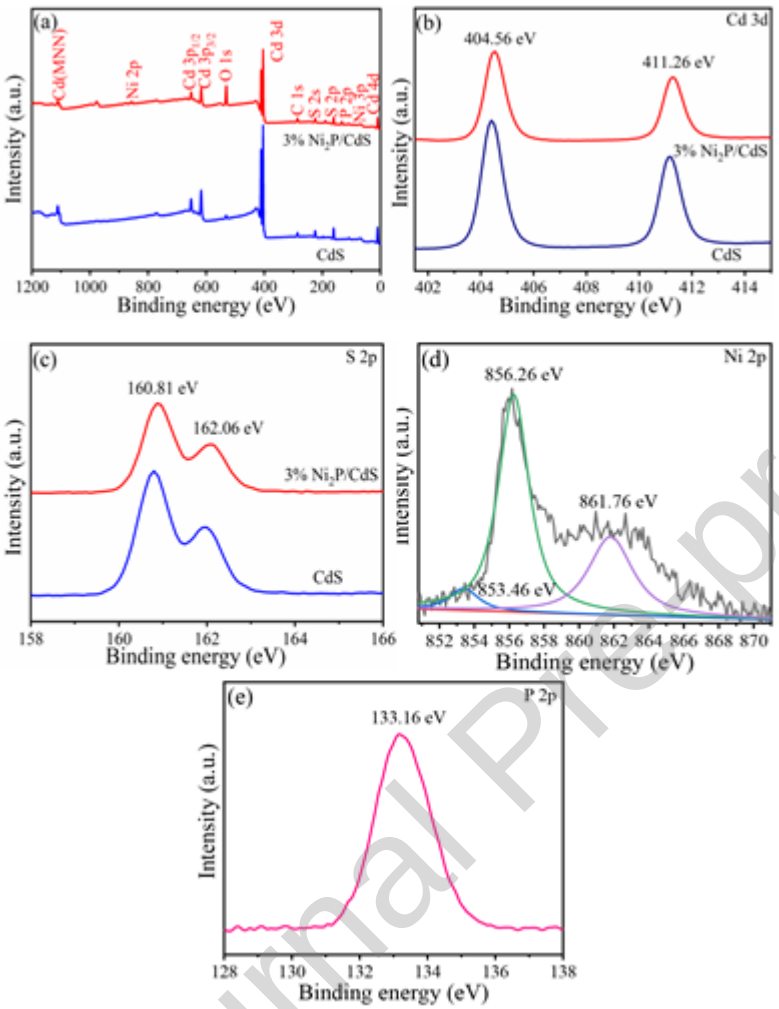

Fig. 3. (a) XPS survey spectra of 3% Ni_2P/CdS. XPS spectra of (b) Cd 3d, (c) S 2p, (d) Ni 2p and (e) P 2p.

The specific surface area, pore and pore size distribution of CdS and 3% Ni_2P/CdS were analyzed by N_2 adsorption-desorption process, and the results are displayed in Fig. 4 and Table 2. As shown in Fig. 4 (a) and 4 (b), CdS and 3% Ni_2P/CdS have class IV isotherms of H3-type hysteresis loops, which are mainly due to the mesopores (2-50 nm) [47]. As illstrated in Table 2, the specific surface area of CdS nanorods and 3% Ni_2P/CdS is 17.34 m^2 /g and 17.21 m^2 /g, respectively, indicating that the growth of spherical granular Ni_2P on CdS nanorods does not change the specific surface area of CdS basically. It also demonstrates that the highly active surface of Ni_2P/CdS can

promote the charge transport and transfer. Compared with CdS nanorods, the average pore size and volume of 3% Ni_2P/CdS are significantly lower, which further vertifys that the gap between the spherical Ni_2P particles and CdS nanorods is filled.

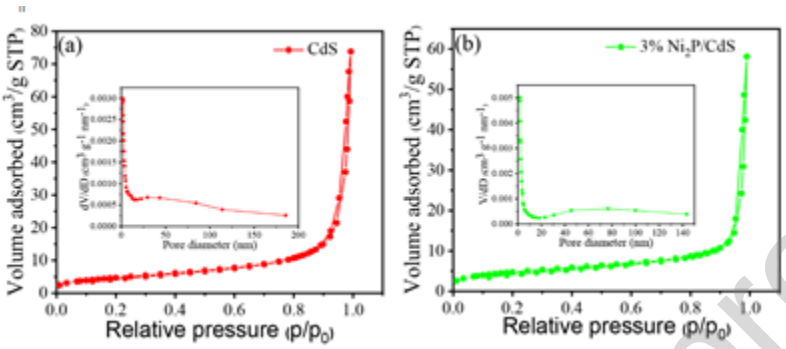

Fig. 4. N_2 absorption-desorption isotherms and pore size distribution of (a) CdS and (b) 3% Ni_2P/CdS.

Table 2. Physical properties of CdS and 3%Ni_2P/CdS.

Samples	**Specific surface area (m^2g^{-1})**	**Average Porediameter (nm)**	**Pore volumes (cm^3g^{-1})**
CdS	17.34	25.41	0.114
3% Ni_2P/CdS	17.21	21.98	0.089

The separation rate of electrons and holes in CdS system after adding Ni_2P was studied by photoluminescence spectroscopy, as shown in Fig. 5. It can be found that under the excitation wavelength of 410 nm, CdS has the highest diffraction peak at 540 nm, and the fluorescence intensity of the sample decreases significantly after the introduction of Ni_2P. This is mainly due to the introduction of Ni_2P promoter, the electrons in CdS conduction band will preferentially transfer to Ni_2P, which reduces the recombination rate of electrons and holes [38].

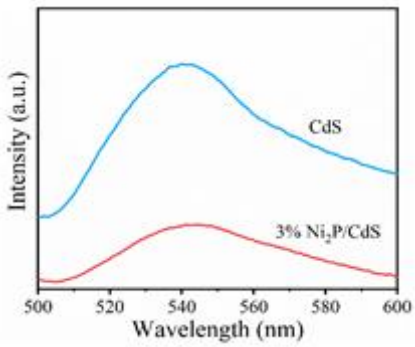

Fig. 5. The PL spectra of CdS and 3% Ni_2P/CdS (λ_{ex}=410 nm).

Fig.6 is UV-vis DRS for CdS, 2%, 3%, 5%, 7% Ni_2P/CdS and Ni_2P. Fig.6 (a) displays that Ni_2P exhibits strong absorption peaks in the range of 300-800 nm, which further proves the metal-like properties. The absorption edge of CdS is about 560 nm, while the absorption edge of 3%, 5%, 7% Ni_2P/CdS is about 600nm, with a red shift of 40 nm. The absorption edge of 2% Ni_2P/CdS is about 580nm, and the red shift is 20 nm. It adminstrates that 2%, 3%, 5%, 7% Ni_2P/CdS has a wider response to the increase of light absorption range in the visible light range, which contributes to the improvement of photocatalytic hydrogen production efficiency. The results manifest that 3% Ni_2P/CdS has a wider range of response to visible light, which contributes to the improvement of photocatalytic hydrogen production efficiency. According to formula (1), the band gap widths of CdS and 3%, 5%, 7% Ni_2P/CdS are 2.37 eV and 2.28 eV respectively, and the band gap width of 2% Ni_2P/CdS is 2.34 eV, as shown in Fig. 6 (b). The decrease of the band gap of Ni_2P/CdS may be due to the introduction of Ni_2P into CdS, and the Ni^{2+} doping in CdS provides the donor energy level [48]. The results indicate that the combination of metal-like cocatalyst Ni_2P reduces the separation distance between electrons and holes in CdS, and reduces the energy required for covalent bond fracture, which is beneficial to the transfer and transmission of photo-generated carriers.

$$(ahv)^{1/n}=A(hv-E_g) \quad (1)$$

(α: Absorption index, h: Planck's constant, v: frequency, A: constant, Eg: band gap width, index n: [direct band gap] n=1/2, [indirect band gap] n=2)

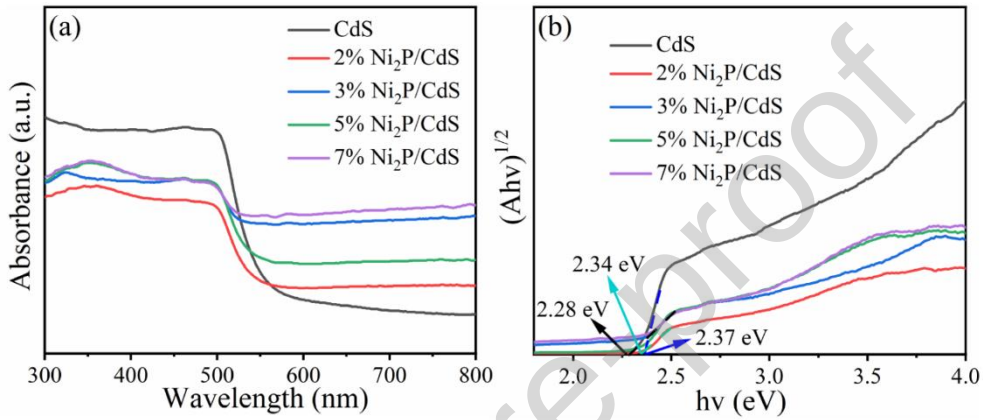

Fig. 6. (a) UV-vis DRS and (b) band gap of CdS and Ni_2P/CdS.

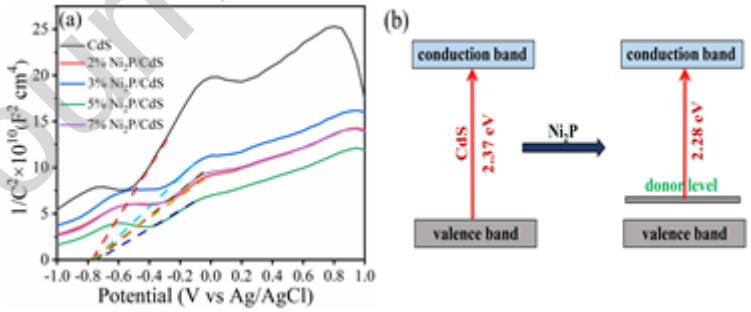

Fig.7. Mott-Schottky plots of CdS and Ni_2P/CdS and (b) donor energy levels formed by Ni_2P doping.

The Mott Schottky curves and energy band changes of CdS, 2%, 3%, 5% and 7% Ni_2P/CdS are shown in Fig. 7. Fig. 7 (a) displays that the slopes of Mott-schottky curves of CdS, 2%, 3%, 5% and 7% Ni_2P/CdS are both positive, revealing the N-type

semiconductor characteristics of CdS. The flat band potentials of CdS and 3% Ni_2P /CdS are about -0.76 V, showing no significant difference. Because the conduction band potential of n-type semiconductor is 0.1 V lower than that of flat band potential, the conduction band potential of CdS and 3% Ni_2P /CdS is -0.86 V [49-51]. After the addition of Ni_2P, the potential of the conduction band of 3% Ni_2P/CdS is basically unchanged, which further proves that Ni_2P acts as a cocatalys. It is similar to the role of precious metal cocatalyst in semiconductors [52]. Fig. 7 (b) illustrates the band change after Ni_2P is added. The results of UV-vis DRS indicate that the band gap of CdS is 2.37 eV. When Ni_2P with metal-like characteristics is recombinated, a donor level above the valence band will be generated due to the doping of residual Ni^{2+} on the surface of Ni_2P/CdS, resulting in the band gap of Ni_2P/CdS being reduced to 2.28 eV. So that CdS has a higher light response under visible light [53].

3.2. Photocatalytic H_2 evolution performance

Fig. 8 is the photocatalytic hydrogen evolution of CdS and Ni_2P/CdS under visible light with Na_2S and Na_2SO_3 as sacrificial agents. Fig. 8 (a) shows hydrogen production of different photocatalysts. The cumulative hydrogen production of Ni_2P/CdS increases linearly with time. 3% Ni_2P/CdS shows the best hydrogen production performance, and the cumulative hydrogen production of 4 h reaches 64 mmol. Fig. 8 (b) displays the rate of hydrogen production of different photocatalysts. Under visible light, the rate of hydrogen production of CdS is only 0.28 mmol $h^{-1}g^{-1}$. The rate of hydrogen production of CdS is not high in visible light, mainly due to photocorrosion and recombination of carriers. After the introduction of cocatalyst Ni_2P, the hydrogen production rate of Ni_2P/CdS increases gradually with the increase of Ni_2P content. When 3% Ni_2P content was added, the hydrogen evolution rate was 16.02 mmol $h^{-1}g^{-1}$, which was 57 times that of CdS, mainly due to the tight interfacial contact promoting electron transfer. With the further increase of Ni_2P content, the hydrogen production rate of Ni_2P/CdS decreases gradually. It is possible that excessive Ni_2P covers the CdS surface and hinders the absorption of light.

Compared with the 3% Ni_2P/CdS prepared by mechanical mixing, the 3% Ni_2P/CdS prepared in this experiment has a tighter contact surface and higher hydrogen production. Comparing the UV-vis DRS and Mott-Schottky of 2% and 3% Ni_2P/CdS can further explain the differences between them, and 3% Ni_2P/CdS can respond better under visible light. With the same conduction band position, the forbidden band width of 3% Ni_2P/CdS is less than 2% Ni_2P/CdS, and the energy required for the separation of electrons and holes is also low, so that electrons can easily enter Ni_2P, and the increase of electrons makes Ni_2P provide more active sites for reduction reaction. Fig. 8 (c) is the hydrogen production rate of 3% Ni_2P/CdS. The hydrogen formation rate of 3% Ni_2P/CdS has no obvious change under visible light, indicating good stability of hydrogen evolution. Fig. 8 (d) shows the XRD pattern of 3% Ni_2P/CdS before and after photocatalysis, indicating that the crystal structure of 3% Ni_2P/CdS does not change after photocatalysis, which further proves that it has excellent photocatalytic stability.

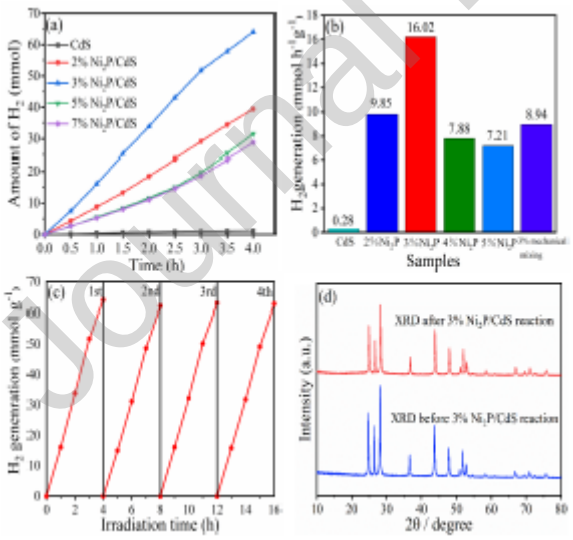

Fig. 8. (a) Photocatalytic H_2 evolution by using the prepared samples under visible light irradiation. (b) The rate of photocatalytic hydrogen on CdS and Ni_2P/CdS with different Ni_2P additions. (c) Recycle runs of H_2 evolution over 3% Ni_2P/CdS. (d) XRD before and after 3% Ni_2P/CdS reaction.

3.3. Interfacial charge separation and the mechanism of photocatalytic H_2 evolution

Fig. 9 illustrates the separation and transition of photogenerated carriers in CdS and 3% Ni_2P/CdS. Fig. 9 (a) is the transient photocurrent diagram of CdS and 3% Ni_2P /CdS. It can be seen that under the same conditions, the current density of 3% Ni_2P /CdS is significantly higher than that of CdS, which indicates that CdS combined with Ni_2P will accelerate the separation rate of electrons and holes. The photocurrent response of 3% Ni_2P/CdS decreased with the increase of radiation time, mainly because the photogenerated carriers in CdS shifted to Ni_2P. Fig. 9 (b) is the electrochemical impedance spectroscopy (EIS) Nyquist plots of CdS and 3% Ni_2P/CdS. The Nyquist radius of 3% Ni_2P/CdS is smaller than that of CdS, indicating that the reduction of interface resistance in 3% Ni_2P/CdS is more conducive to the separation of electrons and holes [54]. It is further proved that CdS combined with Ni_2P can accelerate electron transfer and transmission.

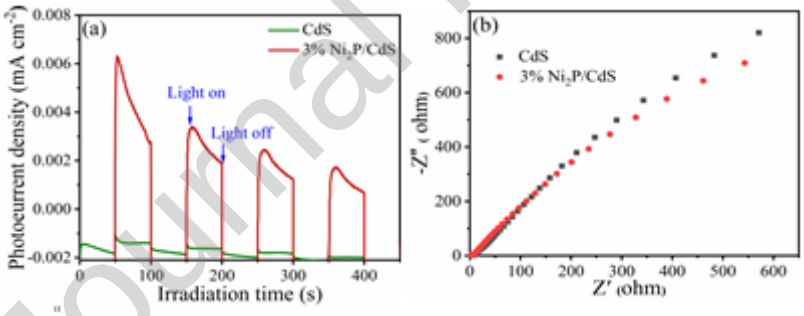

Fig. 9. (a) Photocurrent response of CdS and 3% Ni_2P/CdS and (b) EIS for the Nyquist plots of CdS and 3% Ni_2P/CdS.

Schematic diagram of photocatalytic hydrogen production mechanism of Ni_2P/CdS is illustrated in Fig.10. Spherical granular Ni_2P grows on the surface of CdS nanorods and acts as electron carriers to facilitate the effective separation of CdS electron and hole pairs. Specifically, electrons in the CdS band get excited in visible light and move to the conduction band (CB). The Fermi energy level of CdS is higher than that of Ni_2P, and when Ni_2P is in close contact with CdS, the band is bent [53]. The electrons

excited to the CdS conduction band will be further transferred to Ni_2P, so that the electron hole pair can achieve effective separation, and then generate H_2 through redox reaction. Meanwhile, the holes left in the CdS valence band (VB) are consumed by the sacrificing reagents Na_2S and Na_2SO_3. As a cocatalyst, Ni_2P can act as an electron carrier to inhibit the recombination of electron and hole pairs and provide abundant catalytic active sites for H_2 generation, which can significantly improve the photocatalytic activity of Ni_2P/CdS.

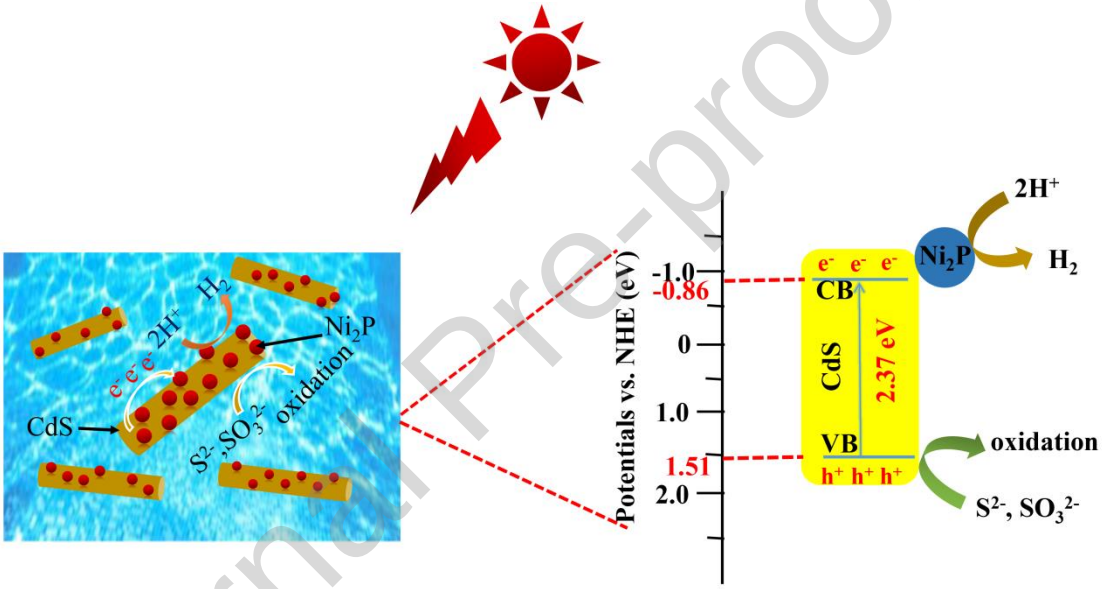

Fig. 10. Schematic diagram of photocatalytic hydrogen production mechanism on Ni_2P/CdS.

4. Conclusions

In summary, the modified impregnation method is proposed as a simple and effective method to prepare compact Ni_2P on the surface of CdS nanorods by in-situ growth. When 3% Ni_2P content was added, the hydrogen evolution rate is 16.02 mmol $h^{-1}g^{-1}$, which was 57 times that of CdS, mainly due to the tight interfacial contact promoting electron transfer. 3% Ni_2P/CdS also shows good stability of hydrogen evolution in cyclic photocatalytic experiments. The interface resistance of 3% Ni_2P/CdS is the lowest, which is conducive to the separation of electrons and holes. As a cocatalyst, Ni_2P can act as an electron carrier to

inhibit the recombination of electron and hole pairs and provide abundant catalytic active sites for H_2 generation, which can significantly improve the photocatalytic activity of Ni_2P/CdS. The separation rate of electrons and holes was verified by PL and electrochemical tests. All characterization results are in good agreement. Furthermore, the possible Mechanism for photocatalytic hydrogen evolution in Ni_2P/CdS system is proposed.

Acknowledgements

The research was supported by Key research and development Program of Anhui Province（Research and industrialization of key technology of color controllable polyurethane-based fluorescent dye), Science and Technology Major Project of Anhui Province, China (No.2021e03020008), Engineering Research Project of Major Scientific and Technological Achievements（No.202103c08020001）, the Natural Science Foundation of Anhui Education Department (No. KJ2020A0473), Hefei Key Technology Major R &D Projects (No. J2019G19) and University Collaborative Innovation Project of Anhui province (GXXT-2019-017).

References

[1] S.E. Hosseini, M.A. Wahid, Hydrogen production from renewable and sustainable energy resources: Promising green energy carrier for clean development, Renew. Sust. Energ. Rev. 57 (2016) 850-866. https://doi.org/10.1016/j.rser.2015.12.112.

[2] H.I. Karunadasa, C.J. Chang, J.R. Long, A molecular molybdenum-oxo catalyst for generating hydrogen from water, Nature 464 (2010) 1329-1333. https://doi.org/10.1038/nature08969.

[3] S. Chen, T. Takata, K. Domen, Particulate photocatalysts for overall water splitting, Nat. Rev. Mater. 2 (2017) 17050. https://doi.org/10.1038/natrevmats.2017.50.

[4] S. Ma, Y. Deng, J. Xie, K. He, W. Liu, X. Chen, X. Li, Noble-metal-free Ni_3C cocatalysts decorated CdS nanosheets for high-efficiency visible-light-driven photocatalytic H_2 evolution Appl. Catal. B Environ.

227 (2018) 218−228. https://doi.org/10.1016/j.apcatb.2018.01.031.

[5] X. Wei, Y. Li, W. Xu, K. Zhang, J. Yin, S. Shi, J. Wei, F. Di, J. Guo, C. Wang, From two-dimensional graphene oxide to three-dimensional honeycomb-like Ni_3S_2@graphene oxide composite: insight into structure and electrocatalytic properties, Roy. Soc. Open Sci. 4 (2017) 171409. https://doi.org/10.1098/rsos.171409.

[6] S. Liang, T. Zhang, D. Zhang, X. Pu, X. Shao, W. Li, J. Dou, One-pot combustion synthesis and efficient broad spectrum photoactivity of Bi/BiOBr:Yb,Er/C photocatalyst, J. Am. Ceram. Soc. 101 (2018) 3424−3436. https://doi.org/10.1111/jace.15520.

[7] W. J. Foo, C. Zhang, G. W. Ho, Non-Noble MetalCu loaded TiO_2 for Enhanced Photocatalytic H_2 Production Nanoscale 5 (2012) 759-764. https://doi.org/10.1039/c2nr33004k.

[8] T. Ruberu, Y. Dong, A. Das, Eisenberg, Richard, E. Photoelectrochemical generation of hydrogen from water using a CdSe quantum dot-sensitized photocathode. ACS Catal. 5 (2015) 2255-2259. https://doi.org/10.1021/cs5021035.

[9] K.C. Christoforidis, Z. Syrgiannis, V.L. Parola, T. Montini, C. Petit, E. Stathatos, R. Godin, J.R. Durrant, M. Prato, P. Fornasiero, Metal-free dual-phase full organic carbon Nanotubes/g-C_3N_4 heteroarchitectures for photocatalytic hydrogen production. Nano Energy 50 (2018) 468-478. https://doi.org/10.1016/j.nanoen.2018.05.070.

[10] T. Muhmood, M. Xia, L. Wu, F. Wang, Under vacuum synthesis of type-I heterojunction between red phosphorus and graphene like carbon nitride with enhanced catalytic, electrochemical and charge separation ability for photodegradation of an acute toxicity category-III compound. ACS Catal. 238 (2018) 568-575. https://doi.org/10.1016/j.apcatb.2018.07.029.

[11] T. Muhmood, M. Xia, L. Wu, F. Wang, Erection of duct-like graphitic carbon nitride with enhanced photocatalytic activity for ACB photodegradation. J. Phys. D: Appl. Phys. 51.6 (2018) 065501. https://doi.org/10.1088/1361-6463/aaa278.

[12] C. Kong, S. Min, G. Lu, Dye-sensitized NiSx catalyst decorated on graphene for highly efficient reduction of water to hydrogen under visible light irradiation. ACS Catal. 4 (2014) 2763-2769. https://doi.org/10.1021/cs5006844.

[13] X. Chen, S. Shen, L. Guo, S.S. Mao, Semiconductor-based photocatalytic hydrogen generation. Chem. Rev. 110 (2010) 6503-6570. https://doi.org/10.1021/cr1001645.

[14] W. Hussain, H. Malik, A. Bahadur, R.A. Hussain, M. Shoaib, S. Iqbal, H. Hussain, I.R. Green, A. Badshah, H. Li, Synthesis and characterization of CdS photocatalyst with different morphologies: visible light activated dyes degradation study, Kinet. Catal. 59 (2018) 710-719. https://doi.org/10.1134/S0023158418060058.

[15] T. Simon, N. Bouchonville, M.J. Berr, A. Vaneski, A. Adrovic, D. Volbers, R. Wyrwich, M. Doblinger, A.S. Susha, A.L. Rogach, F. Jackel, J.K. Stolarczk, J. Feldmann, Redox shuttle mechanism enhances photocatalytic H_2 generation on Ni-decorated CdS nanorods, Nat. Mater. 13 (2014) 1013. https://doi.org/10.1038/nmat4049.

[16] R.M. Irfan, M.H. Tahir, S.A. Khan, M.A. Shaheen, G. Ahmed, S. Iqbal, Enhanced

photocatalytic H_2 production under visible light on composite photocatalyst (CdS/NiSe nanorods) synthesized in aqueous solution, J. Colloid Interface Sci. 557 (2019) 1-9. https://doi.org/10.1016/j.jcis.2019.09.014.

[17] W. Ma, D. Zheng, Y. Xian, X. Hu, Q. Zhang, S. Wang, C. Cheng, J. Liu, P. Wang, Efficient hydrogen evolution under visible light by bimetallic phosphide NiCoP combined with g-C_3N_4/CdS S-scheme heterojunction, ChemCatChem 13 (2021) 4403-4410. https://doi.org/10.1002/cctc.202100833.

[18] D.P. Kumar, E.H. Kim, H. Park, S.Y. Chun, M. Gopannagari, P. Bhavani, D.A. Reddy, J.K. Song, T.K. Kim, Rational synthesis of metal–organic framework-derived noble metal-free nickel phosphide nanoparticles as a highly efficient cocatalyst for photocatalytic hydrogen evolution, ACS Appl. Mater. Interfaces 10 (2018) 26153-26161. https://doi.org/10.1021/acssuschemeng.6b02032.

[19] Y. Li, H. Li, Y. Li, S. Peng, Y. Hu, Fe-B alloy coupled with Fe clusters as an efficient cocatalyst for photocatalytic hydrogen evolution, Chem. Eng. J. 344 (2018) 506-513. https://doi.org/10.1016/j.cej.2018.03.117.

[20] J. Ran, J. Zhang, J. Yu, M. Jaroniec, S.Z. Qiao, Earth-abundant cocatalysts for semiconductor-based photocatalytic water splitting, Chem. Soc. Rev. 43 (2014) 7787-7812. https://doi.org/10.1002/chin.201503290.

[21] P.Y. Kuang, P.X. Zheng, Z.Q. Liu, J.L. Lei, H. Wu, N. Li, T.Y. Ma, Embedding Au quantum dots in rimous cadmium sulfide nanospheres for enhanced photocatalytic hydrogen evolution, Small 12 (2016) 6735–6744. https://doi.org/10.1002/smll.201602870.

[22] G. Han, Y.H. Jin, R.A. Burgess, N.E. Dickenson, X.M. Cao, Y. Sun, Visible-light-driven valorization of biomass intermediates integrated with H_2 production catalyzed by ultrathin Ni/CdS nanosheets, J. Am. Chem. Soc. 139 (2017) 15584-15587. https://doi.org/10.1021/jacs.7b08657.

[23] J. Liu, Q. Jia, J. Long, X. Wang, Z. Gao, Q. Gu, Amorphous NiO as co-catalyst for enhanced visible-light-driven hydrogen generation over g-C_3N_4 photocatalyst, Appl. Catal. B Environ. 222 (2018) 35-43. https://doi.org/10.1016/j.apcatb.2017.09.073.

[24] Z. Yan, X. Yu, A. Han, P. Xu, P. Du, Noble-metal-free $Ni(OH)_2$-Modified CdS/reduced graphene oxide nanocomposite with enhanced photocatalytic activity for hydrogen production under visible light irradiation, J. Phys. Chem. C 118 (2014) 22896-22903. https://doi.org/10.1021/jp5065402.

[25] Y. Chao, J. Zheng, J. Chen, Z. Wang, S. Jia, H. Zhang, Z. Zhu, Highly efficient visible light-driven hydrogen production of precious metal-free hybrid photocatalyst: CdS@NiMoS core–shell nanorods, Catal. Sci. Technol. 7 (2017) 2798-2804. https://doi.org/10.1039/C7CY00964J.

[26] Y. Liu, Y.X. Yu, W.D. Zhang, MoS_2/CdS Heterojunction with high photoelectrochemical activity for H_2 evolution under visible light: the role of MoS_2, J. Phys. Chem. C 117 (2013) 12949-12957. https://doi.org/10.1021/jp4009652.

[27] Z. Pu, Q. Liu, C. Tang, A. M. Asiri, X. Sun, Ni_2P nanoparticle films supported

on a Ti plate as an efficient hydrogen evolution cathode, Nanoscale 6 (2014) 11031−11034. https://doi.org/10.1039/c4nr03037k.

[28] P. Wang, T. Wu, C. Wang, J. Hou, Y. Ao, Combining heterojunction engineering with surface cocatalyst modification to synergistically enhance the photocatalytic hydrogen evolution performance of cadmium sulfide nanorods, ACS Sustainable Chem. Eng. 5 (2017) 7670-7676. https://doi.org/10.1021/acssuschemeng.7b01043.

[29] Y. Liang, Q. Liu, A.M. Asiri, X. Sun, Y. Luo, Self-supported FeP nanorod arrays: a cost-effective 3D hydrogen evolution cathode with high catalytic activity, ACS Catal. 4 (2014) 4065-4069. https://doi.org/10.1021/cs501106g.

[30] Y. Dong, L. Kong, G. Wang, P. Jiang, N. Zhao, H. Zhang, Photochemical synthesis of CoxP as cocatalyst for boosting photocatalytic H_2 production via spatial charge separation, Appl. Catal. B Environ. 211 (2017) 245-251. https://doi.org/10.1016/j.apcatb.2017.03.076.

[31] T. Dong, X. Zhang, P. Wang, H. Chen, P. Yang, Hierarchical nickel-cobalt phosphide hollow spheres embedded in P-doped reduced graphene oxide towards superior electrochemistry activity, Carbon 149 (2019) 222-233. https://doi.org/10.1016/j.carbon.2019.04.050.

[32] W. Zhen, X. Ning, B. Yang, Y. Wu, Z. Li, G. Lu, The enhancement of CdS photocatalytic activity for water splitting via anti-photocorrosion by coating Ni2P shell and removing nascent formed oxygen with artificial gill, Appl. Catal. B Environ. 221 (2018) 243-257. https://doi.org/10.1016/j.apcatb.2017.09.024.

[33] S. Peng, Y. Yang, J. Tan, C. Gan, Y. Li, In situ loading of Ni_2P o n C $d_{0.5}Zn_{0.5}S$ with red phosphorus for enhanced visible light photocatalytic H_2 evolution, Appl. Surf. Sci. 447 (2018) 822-828. https://doi.org/10.1016/j.apsusc.2018.04.050.

[34] P. Ye, X. Liu, J. Iocozzia, Y. Yuan, L. Gu, G. Xu, Z. Lin, A highly stable non-noble metal Ni_2P co-catalyst for increased H_2 generation by g-C_3N_4 under visible light irradiation, J. Mater. Chem. A 5 (2017) 8493–8498. https://doi.org/10.1039/C7TA01031A.

[35] Y. Shi, B. Zhang, Recent advances in transition metal phosphide nanomaterials: synthesis and applications in hydrogen evolution reaction, Chem. Soc. Rev. 45 (2016) 1529-1541. https://doi.org/10.1039/c5cs00434a.

[36] S. Cao, C.J. Wang, W.F. Fu, Y. Chen, Metal phosphides as co-catalysts for photocatalytic and photoelectrocatalytic water splitting, ChemSusChem 10 (2017) 4306–4323. https://doi.org/10.1002/cssc.201701450.

[37] D. Zeng, W.J. Ong, H. Zheng, M. Wu, Y. Chen, D.L. Peng, M.Y. Han, $Ni_{12}P_5$ nanoparticles embedded into porous g-C_3N_4 nanosheets as a noble-metal-free hetero-structure photocatalyst for efficient H_2 production under visible light, J. Mater. Chem. A 5 (2017) 16171-16178. https://doi.org/10.1039/C7TA04816E.

[38] Z. Sun, M. Zhu, M. Fujitsuka, A. Wang, C. Shi, T. Majima, Phase Effect of Ni_xP_y Hybridized with g-C_3N_4 for Photocatalytic Hydrogen Generation, ACS Appl. Mater. Interfaces 9 (2017) 30583-30590. https://doi.org/10.1021/acsami.7b06386.

[39] D.P. Kumar, J. Choi, S. Hong, D.A. Reddy, S. Lee, T.K. Kim, Rational synthesis of metal–organic framework-derived noble metal-free nickel phosphide nanoparticles as a highly efficient cocatalyst for photocatalytic hydrogen evolution, ACS Sustainable Chem. Eng. 4 (2016) 7158-7166. https://doi.org/10.1021/acssuschemeng.6b02032.

[39] J.S. Jang, U.A. Joshi, J.S. Lee, Solvothermal synthesis of CdS nanowires for photocatalytic hydrogen and electricity production, J. Phys. Chem. C 111 (2007) 13280-13287. https://doi.org/10.1021/jp072683b.

[40] C. Ye, J. Li, Z. Li, X. Li, X. Fan, L. Zhang, B. Chen, C. Tung, L. Wu, Enhanced driving force and charge separation efficiency of protonated g-C_3N_4 for photocatalytic O_2 evolution, ACS Catal. 5 (2015) 6973-6979. https://doi.org/10.1021/acscatal.5b02185.

[41] A.V. Okotrub, I.P. Asanov, S.V. Larionov, A.G. Kudashov, T.G. Leonova, L.G. Bulusheva, Growth of CdS nanoparticles on the aligned carbon nanotubes, Phys. Chem. Chem. Phys. 12 (2010) 10871-10875. https://doi.org/10.1039/c000189a.

[42] X. Fu, L. Zhang, L. Liu, H. Li, S. Meng, X. Ye, S. Chen, In situ photodeposition of MoSx on CdS nanorods as a highly efficient cocatalyst for photocatalytic hydrogen production, J. Mater. Chem. A 5 (2017) 15287–15293. https://doi.org/10.1039/C7TA04814A.

[43] Y. Xue, Q. Guan, W. Li, Synthesis of bulk and supported nickel phosphide using microwave radiation for hydrodeoxygenation of methyl palmitate, RSC Adv. 5 (2015) 53623-53628. https://doi.org/10.1039/C5RA09020B.

[44] D.A. Reddy, H.K. Kim, Y. Kim, S. Lee, J. Choi, M.J. Islam, D.P. Kumar, T.K. Kim, Multicomponent transition metal phosphides derived from layered double hydroxide double-shelled nanocages as an efficient non-precious co-catalyst for hydrogen production, J. Mater. Chem. A 4 (2016) 13890-13898. https://doi.org/10.1039/C6TA05741A.

[45] X. Liu, X. Li, L. Qin, J. Mu, S.Z. Kang, Dramatic enhancement of the photocatalytic activity of $Cd_{0.5}Zn_{0.5}S$ nanosheets via phosphorization calcination for visible-light-driven H_2 evolution, J. Mater. Chem. A 5 (2017) 14682-14688. https://doi.org/10.1039/C7TA04589A.

[46] X. Liu, A.L. Jin, Y.S. Jia, T.L. Xia, C.X. Deng, M.H. Zhu, Synergy of adsorption and visible-light photocatalytic degradation of methylene blue by a bifunctional Z-scheme heterojunction of WO_3/g-C_3N_4, Appl. Surf. Sci. 405 (2017) 359-371. https://doi.org/10.1016/j.apsusc.2017.02.025.

[47] Z. Fang, L. Peng, Y. Qian, X. Zhang, Y. Xie, J. Cha, G. Yu, Dual tuning of Ni-Co-A (A=P, Se, O) nanosheets by anion substitution and holey engineering for efficient hydrogen evolution, J. Am. Chem. Soc. 140 (2018) 5241-5247. https://doi.org/10.1021/jacs.8b01548.

[48] D.P. Kumar, S. Hong, D.A. Reddy, T.K. Kim, Noble metal-free ultrathin MoS_2 nanosheet-decorated CdS nanorods as an efficient photocatalyst for spectacular hydrogen evolution under solar light irradiation, J. Mater. Chem. A 4 (2016) 18551-18558. https://doi.org/10.1039/C6TA08628D.

[50] J. Zhong, Y. Zhang, C. Hu, R. Hou, H. Yin, H. Li, Y. Huo, Supercritical solvothermal preparation of a $Zn_xCd_{1-x}S$ visible photocatalyst with enhanced

activity, J. Mater. Chem. A 2 (2014) 19641-19647. https://doi.org/10.1039/C4TA04021J.

[51] Z. Wang, Z. Qi, X. Fan, D. Y. C. Leung, J. Long, Z. Zhang, T. Miao, S. Meng, S. Chen, X. Fu, Intimately contacted Ni_2P on CdS nanorods for highly efficient photocatalytic H_2 evolution: new phosphidation route and the interfacial separation mechanism of charge carriers, Appl. Catal. B Environ. 281 (2021) 119443. https://doi.org/10.1016/j.apcatb.2020.119443.

[52] J. Choi, D. Amaranatha Reddy, N.S. Han, S. Jeong, S. Hong, D. Praveen Kumar, J.K. Song, T.K. Kim, Modulation of charge carrier pathways in CdS nanospheres by integrating MoS_2 and Ni_2P for improved migration and separation toward enhanced photocatalytic hydrogen evolution, Catal. Sci. Technolog. 7 (2017) 641-649. https://doi.org/10.1039/C6CY02145J.

[53] X. Chen, S. Shen, L. Guo, S. S. Mao, Semiconductor-based photocatalytic hydrogen generation, Chem.Rev.110 (2010) 6503-6570. https://doi.org/10.1021/cr1001645.

[54] R. Wei, Z. Huang, G. Gu, Z. Wang, L. Zeng, Y. Chen, Z. Liu, Dual-cocatalysts decorated rimous CdS spheres advancing highly-efficient visible-light photocatalytic hydrogen production, Appl. Catal. B Environ. 231 (2018) 101-107. https://doi.org/10.1016/j.apcatb.2018.03.014.

Declaration of interests

☒ The authors declare that they have no known competing financial interests or personal relationships that could have appeared to influence the work reported in this paper.

☐The authors declare the following financial interests/personal relationships which may be considered as potential competing interests:

CRediT author statement

TABLE 1 Contributor Roles Taxonomy (CRediT).

Author	contributions
Wangyang Ma	Synthesis, device fabrication, device characterization, optimization, and writing original draft
Dewen Zheng	Investigation, Validation, Formal analysis, Data curation, Writing - original draft.

Bihua Xiao	Formal analysis, Investigation.
Yuxi Xian	Resources, Writing - review and editing, Funding acquisition.
Qian Zhang	Formal analysis, Validation.
Shanyu Wang	Formal analysis, Data curation.
Jin Liu	Conceptualization, Methodology, Formal analysis, Data curation, Resources,
Ping Wang	Characterization, data analysis, and methodology.
Xianhai Hu	Writing - review and editing, Supervision, Project administration, Funding acquisition.

Graphical abstract

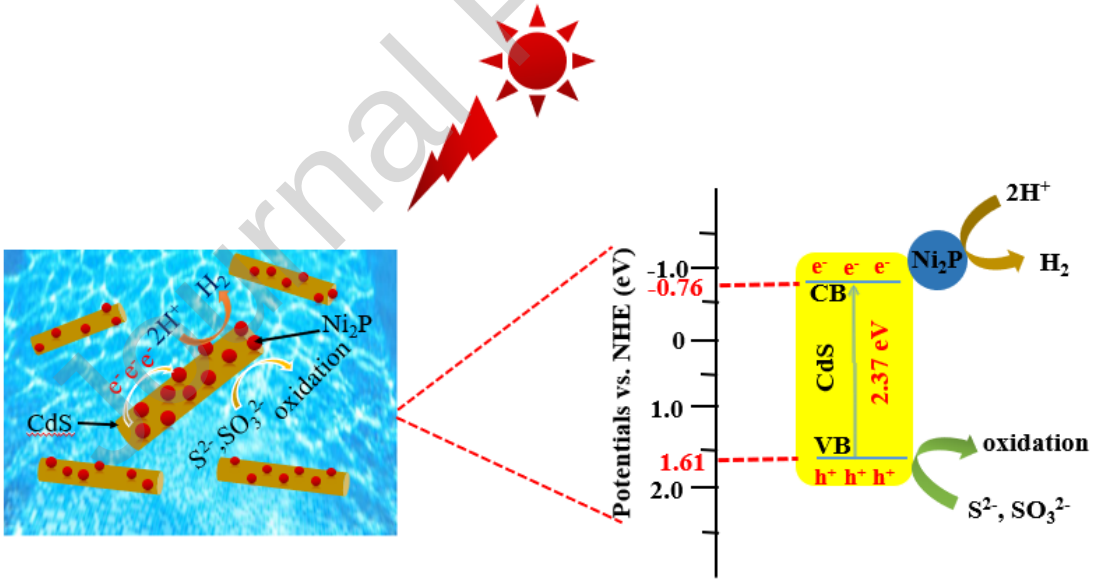

Ni_2P /CdS was prepared by in-situ growth of Ni_2P cocatalyst on the CdS surface using the modified impregnation method. The hydrogen production rate of Ni_2P/CdS reached an astonishing 16.02 mmol $h^{-1}g^{-1}$, which was 57 times that of CdS.

Highlights

1. A simple and effective method to combine the main catalyst and the cocatalyst by a

modified impregnation method is provided.

2. Ni_2P, as an electron carrier, can effectively promote the separation of electrons and holes, and significantly improve the photocatalytic activity of Ni_2P/CdS.
3. The photocatalytic hydrogen evolution rate of 3%Ni_2P/CdS is 57 times that of CdS. Moreover, Ni_2P/CdS photocatalyst has outstanding stability for hydrogen production.